

# A Viscoelastic-Viscoplastic Combined Constitutive Model for Thermoplastic Resins

Seishiro Matsubara and Kenjiro Terada

**Abstract** A viscoelastic-viscoplastic combined constitutive model is presented to represent large deformations of amorphous thermoplastic resins. The model is endowed with viscoelastic and viscoplastic rheology elements connected in series. The standard generalized Maxwell model is used to determine the stress and characterize the viscoelastic material behavior at small or moderate strain regime. To realize the transient creep deformations along with kinematic hardening due to frictional resistance and orientation of molecular chains, a proven finite strain viscoplastic model is employed. After identifying the material parameters with reference to experimental data, we verify and demonstrate the fundamental performances of the proposed model in reproducing typical material behavior of resin.

## 1 Introduction

Thermoplastic resins are known to exhibit peculiar material behavior. Early researches were inspired by the work done by Eyring [10] who studied it physicochemically based on reaction kinetics of molecular chains. Among them, Argon's double kink hypothesis [5, 6], which is based on disclination loop theory Li and Gilman [21], has been widely used for the viscoplastic multiplier in various constitutive models for thermoplastic resins to represent the initial yielding at a moderate deformation regime; see also Liu and Li [22] in this context. With the help of high-performance of computational resource, these early theoretical developments enjoys the fruits of computational plasticity [26] in representing complex material behavior and accelerates further elaboration of material models for thermoplastic resins.

---

S. Matsubara

Department of Civil Engineering, Tohoku University, Sendai, Japan

e-mail: seishiro.matsubara.t4@dc.tohoku.ac.jp

K. Terada (✉)

International Research Institute of Disaster Science, Tohoku University,  
Sendai, Japan

e-mail: tei@irides.tohoku.ac.jp

Boyce et al. [8] proposed a phenomenological constitutive model that can successfully represent the stress-softening behavior after initial yielding by introducing pressure dependency and evolution of shear yield strength into the Argon's model [6]. This model is extended by Wu and Giessen [31, 32] to reproduce shear bands and necking phenomena at a moderate deformation regime. Also, based on the Boyce's theory, Anand and Gurtin [4] provide a model within the thermodynamics framework that represents smooth transition from the initial yielding to stress-softening in consideration of the evolution of free volume in the viscoplastic deformations. Moreover, Fleischhauer et al. [11] extend the models developed by Mulliken et al. [23] and Dupaix and Boyce [9] and propose a rheology model involving a viscoplastic element connected with a Langevin element in parallel to represent compressive material behavior of both thermosetting and thermoplastic resins.

Apart from the Argon's framework [5, 6], the cooperative model, which is developed by Richeton et al. [27–29] based on the model introduced by Fotheringham and Cherry [13], is worthy of attention. By extending the cooperative model, Anand et al. [3] and Ames et al. [2] propose phenomenological models within the thermodynamics framework, which incorporate the viscoplastic defect energy to represent the dynamic recovery behavior during unloading. The extension of these models, which is proposed by Srivastava et al. [30], is a rheology model composed of multiple viscoplastic elements to adjust for the material behavior above a glass-transition temperature. This model enables us to work with the change of physical properties around the glass-transition temperature, but entails a bunch of parameters and seems to be remotely related to physical ground. In the meantime, according to Aleksy et al. [1] and Kermouche et al. [18], glassy thermoplastic resins behave as a viscoelastic material in small and moderately large deformation regimes, whereas the viscoplastic behavior tends to be dominant in a large deformation regime. Surprisingly few studies have so far been made at the constitutive modeling in this context, though there seem to be some models representing the coupling between viscoelastic and viscoplastic material responses; see, e.g., Nedjar [24, 25].

To encompass various material responses depending on different amounts of deformation, the article presents a new rheology-based constitutive model for glassy amorphous thermoplastic resins that is composed of viscoelastic and viscoplastic elements in series. The distinct feature of the proposed model is that the elastic elements are installed in the viscoelastic part only so that the viscoplastic part is not directly related to the stress. Also, thanks to the series combination, three types of rheology elements are introduced in the model to represent different characteristic features of the material behavior according to the amount of deformation. Specifically, the uniform creep behavior in a small deformation regime is represented by the standard generalized Maxwell model [15, 16]. Two sets of rheology elements are connected in parallel to construct the viscoplastic part of the model. One of them is composed of serially connected frictional slider-dumper element to represent non-uniform creep deformation along with the initial yielding followed by stress-softening in a moderately large deformation regime. In this study, the model proposed by Boyce et al. [8] is employed for this part. The other is a special type of spring elements introduced by Ames et al. [2] to represent the orientation hardening

in a large deformation regime. As a ground for the argument of such a viscoelastic and viscoplastic combination in series, we start the formulation with the first and second laws of thermodynamics. The experimental data for polymethylmethacrylate (PMMA) available in the literature are used to identify the material parameters and the fundamental performances of the proposed model in reproducing typical material behavior of resin are verified and demonstrated with simple numerical examples.

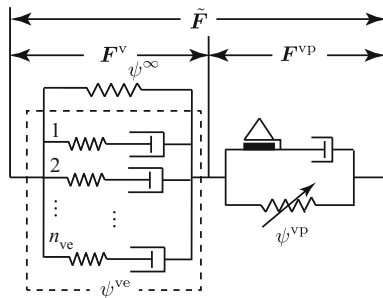
## 2 A Viscoelastic-Viscoplastic Combined Constitutive Law

This section is devoted to the formulation of the viscoelastic-viscoplastic combined constitutive law within the finite strain framework. Thermomechanical deformation is also considered without loss of generality, but isotropy is assumed for both the thermal and mechanical deformations in this study.

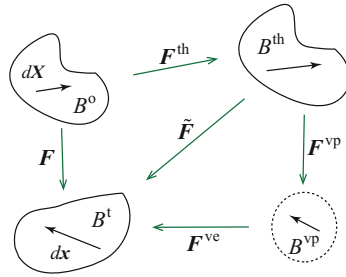
### 2.1 Kinematic Variables

Figure 1 shows the rheology model corresponding to the constitutive law proposed in this study. The model is composed of viscoelastic and viscoplastic parts connected in series, each of which corresponds to viscoelastic and viscoplastic components,  $F^{ve}$  and  $F^{vp}$ , obtained as a result of the following multiplicative decomposition of the mechanical deformation gradient  $\tilde{F}$  with reference to the initial, thermally dilated, viscoplastic (intermediate) and current configurations depicted in Fig. 2 along the line of Kröner [19] and Lee [20]:

$$\tilde{F} = F^{ve} F^{vp} \tag{1}$$



**Fig. 1** Rheology model of coupled viscoelasticity with viscoplasticity. The model combines a viscoplastic element with a generalized Maxwell model in series and necessitates the multiplicative decomposition of the deformation gradient into viscoelastic and viscoplastic ones. The total stress is determined only with the generalized Maxwell model



**Fig. 2** Configurations associated with multiplicative decomposition of deformation gradient;  $B^{vp}$ : viscoelastically unloaded configuration with viscoplastic deformation gradient  $F^{vp}$ ; thermally dilated configuration  $B^{th}$ ; current configuration  $B^t$  with viscoelastic deformation gradient  $F^{ve}$

Here, the total deformation gradient is expressed as

$$F = \tilde{F}F^{th} \tag{2}$$

with  $F^{th}$  being the thermal deformation gradient, which, due to isotropy, can be expressed as

$$F^{th} = (1 + \alpha_t \theta)\mathbf{1} \tag{3}$$

where  $\mathbf{1}$  is the second-order identify tensor,  $\theta$  is the change in temperature and  $\alpha_t$  is the coefficient of thermal expansion (CTE).

The viscoelastic part of this rheology model corresponds to a finite strain version of the generalized Maxwell elements, whereas the viscoplastic part covers a lot of ground for corresponding constitutive models. However, the spring element set in parallel with the serially connected frictional slider-dumper element is worthy of attention, as the back stress due to orientation hardening is developed in it after the expansion according to the viscoplastic deformation. In what follows, kinematic variables necessary in the formulation are defined based on the multiplicative decomposition introduced above.

The mechanical deformation gradient  $\tilde{F}$  can be decomposed into the volumetric and isochoric components,  $J^{\frac{1}{3}}$  and  $\bar{F}$ , as

$$\tilde{F} = J^{\frac{1}{3}}\bar{F} \tag{4}$$

where  $J := \det(\tilde{F})$  [12]. These volumetric and isochoric components can also be decomposed into viscoelastic and viscoplastic parts as

$$J = J^{ve}J^{vp}, \quad \text{and} \quad \bar{F} = \bar{F}^{ve}\bar{F}^{vp} \tag{5}$$

where we have defined  $J^{\text{ve}} := \det(\mathbf{F}^{\text{ve}})$  and  $J^{\text{vp}} := \det(\mathbf{F}^{\text{vp}})$ . In this study, incompressibility is assumed for the viscoplastic deformation so that  $J^{\text{vp}} = 1$ , from which (5)<sub>1</sub> and (1) yields  $J = J^{\text{ve}}$  and  $\tilde{\mathbf{F}} = \mathbf{F}^{\text{ve}}\bar{\mathbf{F}}^{\text{vp}}$ , respectively.

The right Cauchy-Green and left Cauchy-Green tensors associated with the mechanical deformation are given as  $\tilde{\mathbf{C}} = (\bar{\mathbf{F}}^{\text{vp}})^{\text{T}} \mathbf{C}^{\text{ve}} \bar{\mathbf{F}}^{\text{vp}}$  and  $\tilde{\mathbf{b}} = \mathbf{F}^{\text{ve}} \bar{\mathbf{b}}^{\text{vp}} (\mathbf{F}^{\text{ve}})^{\text{T}}$ . Here,  $\mathbf{C}^{\text{ve}}$  and  $\bar{\mathbf{b}}^{\text{vp}}$  are the viscoelastic right Cauchy-Green and viscoplastic left Cauchy-Green tensors that have respectively been defined as

$$\mathbf{C}^{\text{ve}} = (\mathbf{F}^{\text{ve}})^{\text{T}} \mathbf{F}^{\text{ve}} \quad \text{and} \quad \bar{\mathbf{b}}^{\text{vp}} = \bar{\mathbf{F}}^{\text{vp}} (\bar{\mathbf{F}}^{\text{vp}})^{\text{T}} \quad (6)$$

Also, the mechanical velocity gradient can be additively decomposed as

$$\tilde{\mathbf{l}} = \dot{\tilde{\mathbf{F}}}\tilde{\mathbf{F}}^{-1} = \mathbf{l}^{\text{ve}} + \mathbf{F}^{\text{ve}}\bar{\mathbf{l}}^{\text{vp}}(\mathbf{F}^{\text{ve}})^{-1} \quad (7)$$

where we have respectively defined the viscoelastic and viscoplastic velocity gradients referring to the viscoelastically unloaded configuration  $B^{\text{vp}}$  as  $\mathbf{l}^{\text{ve}} = \dot{\mathbf{F}}^{\text{ve}} (\mathbf{F}^{\text{ve}})^{-1}$  and  $\bar{\mathbf{l}}^{\text{vp}} = \dot{\bar{\mathbf{F}}}^{\text{vp}} (\bar{\mathbf{F}}^{\text{vp}})^{-1}$ . Each of these velocity gradients can be decomposed into the symmetric and anti-symmetric parts as

$$\tilde{\mathbf{l}} = \text{sym} [\tilde{\mathbf{l}}] + \text{skew} [\tilde{\mathbf{l}}] = \tilde{\mathbf{d}} + \tilde{\mathbf{w}}, \quad (8)$$

$$\bar{\mathbf{l}}^{\text{vp}} = \text{sym} [\bar{\mathbf{l}}^{\text{vp}}] + \text{skew} [\bar{\mathbf{l}}^{\text{vp}}] = \bar{\mathbf{d}}^{\text{vp}} + \bar{\mathbf{w}}^{\text{vp}}, \quad (9)$$

$$\mathbf{l}^{\text{ve}} = \text{sym} [\mathbf{l}^{\text{ve}}] + \text{skew} [\mathbf{l}^{\text{ve}}] = \mathbf{d}^{\text{ve}} + \mathbf{w}^{\text{ve}} \quad (10)$$

where  $\text{sym}[\bullet]$  and  $\text{skew}[\bullet]$  are the symmetric and anti-symmetric parts of a second-order tensor  $\bullet$ .

We assume that the viscoplastic deformation of thermoplastic resins is affine so that the mapping between viscoelastically unloaded configuration  $B^{\text{vp}}$  and current configuration  $B^{\text{t}}$  is irrotational (as suggest by Boyce et al. [8]) as  $\mathbf{R}^{\text{ve}} = \mathbf{1}$  and  $\mathbf{w}^{\text{ve}} = \mathbf{0}$ . This assumption postulates that the flow direction of the viscoplastic permanent deformation in current configuration  $B^{\text{t}}$  be coincident with the slip direction of molecular chains. In this case, the second term of the right-hand side of (7) becomes  $\mathbf{F}^{\text{ve}}\bar{\mathbf{l}}^{\text{vp}}(\mathbf{F}^{\text{ve}})^{-1} = \mathbf{V}^{\text{ve}}\bar{\mathbf{l}}^{\text{vp}}(\mathbf{V}^{\text{ve}})^{-1} = \bar{\mathbf{l}}^{\text{vp}}$  so that  $\tilde{\mathbf{l}} = \mathbf{l}^{\text{ve}} + \bar{\mathbf{l}}^{\text{vp}}$ . Therefore, with (10), we have  $\tilde{\mathbf{d}} = \mathbf{d}^{\text{ve}} + \bar{\mathbf{d}}^{\text{vp}}$  and  $\tilde{\mathbf{w}} = \bar{\mathbf{w}}^{\text{vp}}$ .

## 2.2 Free Energy

The total free energy  $\psi$  for the material under consideration is defined as

$$\psi = \psi^{\text{th}}(\mathbf{F}^{\text{th}}, \theta) + \psi^{\text{ve}}(\tilde{\mathbf{C}}, \bar{\mathbf{F}}^{\text{vp}}, \mathbf{I}^{\alpha}, \theta) + \psi^{\text{vp}}(\bar{\mathbf{b}}^{\text{vp}}, \theta) \quad (11)$$

where  $\psi^{\text{th}}$  and  $\psi^{\text{ve}}$  are the free energies for thermal, viscoelastic-viscoplastic deformations [15, 16], respectively, and  $\psi^{\text{vp}}$  is the defect energy associated with viscoplastic deformation [4]. Here,  $\mathbf{\Gamma}^\alpha$  ( $\alpha = 1, \dots, n_{\text{ve}}$ ) are thermodynamic strains of rheology elements referring to viscoelastically unloaded configuration  $B^{\text{vp}}$ .

In consideration of stress-free dilation volume  $\mathbf{p}^{\text{th}} = -\frac{\partial\psi^{\text{th}}}{\partial\mathbf{F}^{\text{th}}} = \mathbf{0}$ , the material time derivative of the total free energy  $\psi$  becomes

$$\dot{\psi} = \frac{\partial\psi^{\text{ve}}}{\partial\tilde{\mathbf{C}}} : \dot{\tilde{\mathbf{C}}} + \frac{\partial\psi^{\text{ve}}}{\partial\bar{\mathbf{F}}^{\text{vp}}} : \dot{\bar{\mathbf{F}}^{\text{vp}}} + \frac{\partial\psi^{\text{vp}}}{\partial\bar{\mathbf{F}}^{\text{vp}}} : \dot{\bar{\mathbf{F}}^{\text{vp}}} + \sum_{\alpha=1}^{n_{\text{ve}}} \frac{\partial\psi^{\text{ve}}}{\partial\mathbf{\Gamma}^\alpha} : \dot{\mathbf{\Gamma}}^\alpha + \frac{\partial\psi}{\partial\theta} \dot{\theta} \quad (12)$$

in which the 2nd Piola-Kirchhoff stress and the entropy density can be identified as

$$\mathbf{S} = 2\rho_0 \frac{\partial\psi^{\text{ve}}}{\partial\tilde{\mathbf{C}}} \quad \text{and} \quad \eta = -\frac{\partial\psi}{\partial\theta}. \quad (13)$$

Here,  $\rho_0$  is the initial mass density. Then, applying the 1st and 2nd laws of thermodynamics along with (12), we have the internal or intrinsic dissipation energy referring to the thermally dilated configuration  $B^{\text{th}}$ , as

$$\begin{aligned} \phi_{\text{internal}} &= \frac{1}{2} \mathbf{S} : \dot{\tilde{\mathbf{C}}} - \rho_0 (\dot{\psi} + \dot{\theta}\eta) \\ &= -\rho_0 \frac{\partial\psi^{\text{ve}}}{\partial\bar{\mathbf{F}}^{\text{vp}}} : \dot{\bar{\mathbf{F}}^{\text{vp}}} - \rho_0 \frac{\partial\psi^{\text{vp}}}{\partial\bar{\mathbf{F}}^{\text{vp}}} : \dot{\bar{\mathbf{F}}^{\text{vp}}} - \sum_{\alpha=1}^{n_{\text{ve}}} \rho_0 \frac{\partial\psi^{\text{ve}}}{\partial\mathbf{\Gamma}^\alpha} : \dot{\mathbf{\Gamma}}^\alpha \end{aligned} \quad (14)$$

where the sum of the first and second terms of the right-hand side is the viscoplastic dissipation energy density and the third term represents the viscoelastic dissipation energy density.

### 2.3 Viscoelastic Rheology Element

The viscoelastic part of the rheology element is formulated based on the theory presented by Holzapfel et al. [15, 16]. First, we introduce the following form of the viscoelastic-viscoplastic coupled free energy density:

$$\rho_0\psi^{\text{ve}} = \rho_0\psi^\infty + \sum_{\alpha=1}^{n_{\text{ve}}} \left[ \mathbf{\Gamma}^\alpha : \mathbb{C}^\alpha : \mathbf{\Gamma}^\alpha - 2\rho_0 \frac{\partial\psi^\alpha}{\partial\mathbf{C}^{\text{ve}}} : \mathbf{\Gamma}^\alpha + \rho_0\psi^\alpha \right] \quad (15)$$

where  $\psi^\infty = \psi^\infty(\tilde{\mathbf{C}}, \bar{\mathbf{F}}^{\text{vp}}, \theta)$  is the free energy density of the purely elastic element. Also,  $\psi^\alpha = \psi^\alpha(\tilde{\mathbf{C}}, \bar{\mathbf{F}}^{\text{vp}}, \theta)$  is the ideally elastic energy density of Maxwell elements, each which is virtually defined as the elastic stored energy during the relaxation process. Furthermore,  $\mathbb{C}^\alpha = \mathbb{C}^\alpha(\tilde{\mathbf{C}}, \bar{\mathbf{F}}^{\text{vp}}, \theta)$  is a positive definite fourth-order tensor introduced for each Maxwell element, which has the same unit with that of the elastic moduli tensor.

With this definition of the free energy density  $\psi^{ve}$ , Eq. (13) becomes

$$\mathbf{S} = 2\rho_0 \frac{\partial \psi^{ve}}{\partial \tilde{\mathbf{C}}} = (\mathbf{F}^{vp})^{-1} \left[ 2\rho_0 \frac{\partial \psi^{ve}}{\partial \mathbf{C}^{ve}} \right] (\mathbf{F}^{vp})^{-T} = (\mathbf{F}^{vp})^{-1} \mathbf{H} (\mathbf{F}^{vp})^{-T} \quad (16)$$

which defines the 2nd Piola-Kirchhoff stress referring thermally dilated configuration  $B^{th}$ . Here, we have defined the thermodynamic non-equilibrated stress that refers to viscoelastically unloaded configuration  $B^{vp}$  as

$$\begin{aligned} \mathbf{H} &= 2\rho_0 \frac{\partial \psi^{ve}}{\partial \mathbf{C}^{ve}} \\ &= 2\rho_0 \frac{\partial \psi^\infty}{\partial \mathbf{C}^{ve}} + \sum_{\alpha=1}^{n_{ve}} \left[ \Gamma^\alpha : 2 \frac{\partial \mathbf{C}^\alpha}{\partial \mathbf{C}^{ve}} : \Gamma^\alpha - 2 \frac{\partial \mathbf{H}^\alpha}{\partial \mathbf{C}^{ve}} : \Gamma^\alpha + 2\rho_0 \frac{\partial \psi^\alpha}{\partial \mathbf{C}^{ve}} \right] \\ &= \mathbf{H}^\infty + \sum_{\alpha=1}^{n_{ve}} \left[ \Gamma^\alpha : 2 \frac{\partial \mathbf{C}^\alpha}{\partial \mathbf{C}^{ve}} : \Gamma^\alpha - 4\rho_0 \frac{\partial^2 \psi^\alpha}{\partial \mathbf{C}^{ve} \partial \mathbf{C}^{ve}} : \Gamma^\alpha + \mathbf{H}^\alpha \right] \end{aligned} \quad (17)$$

along with the viscoelastic thermodynamic strain  $\Gamma^\alpha$ . Here,  $\mathbf{H}^\infty$  and  $\mathbf{H}^\alpha$  have been defined as

$$\mathbf{H}^\infty = 2\rho_0 \frac{\partial \psi^\infty}{\partial \mathbf{C}^{ve}} \quad \text{and} \quad \mathbf{H}^\alpha = 2\rho_0 \frac{\partial \psi^\alpha}{\partial \mathbf{C}^{ve}}. \quad (18)$$

In this study, we employ the following St. Venant-Kirchhoff hyperelastic strain energy for the free energy of the purely elastic element in the generalized Maxwell model:

$$\rho_0 \psi^\infty = \frac{1}{2} K^\infty [\text{tr}(\mathbf{E}^{ve})]^2 + G^\infty [\text{dev}(\mathbf{E}^{ve}) : \text{dev}(\mathbf{E}^{ve})] \quad (19)$$

so that the stress in the purely elastic element referring to the viscoelastically unloaded configuration  $B^{vp}$  yields

$$\mathbf{H}^\infty = K^\infty \text{tr}(\mathbf{E}^{ve}) \mathbf{1} + 2G^\infty \text{dev}(\mathbf{E}^{ve}) \quad (20)$$

where viscoelastic Green strain  $\mathbf{E}^{ve}$  is expressed as  $\mathbf{E}^{ve} = \frac{1}{2} (\mathbf{C}^{ve} - \mathbf{1})$  using the right-Cauchy-Green viscoelastic deformation tensor  $\mathbf{C}^{ve}$  in (6). Also,  $K^\infty$  and  $G^\infty$  are equivalent to the bulk and shear moduli.

We postulate that the ideal elastic free energy of each Maxwell element (15) be proportional to the purely elastic free energy as  $\psi^\alpha = \gamma^\alpha \psi^\infty$  so that the stress referring to viscoelastically unloaded configuration  $B^{vp}$  becomes

$$\mathbf{H}^\alpha = 2\rho_0 \frac{\partial \psi^\alpha}{\partial \mathbf{C}^{ve}} = \gamma^\alpha \mathbf{H}^\infty \quad (21)$$

where  $\gamma^\alpha \in (0, 1]$  is the relative elastic modulus defined as  $\gamma^\alpha = \frac{E^\alpha}{E^\infty}$ . Here,  $E^\alpha$  and  $E^\infty$  are Young's moduli of each Maxwell element and of the purely elastic element.

Also, by defining the tangent modulus of each Maxwell element as

$$\mathbb{D}^\alpha = 4\rho_0 \frac{\partial^2 \psi^\alpha}{\partial \mathbf{C}^{\text{ve}} \partial \mathbf{C}^{\text{ve}}} = \gamma^\alpha (K^\infty \mathbf{I}^{\text{sym}} + 2G^\infty \mathbf{I}^{\text{dev}}) \quad (22)$$

we assume that the fourth-order modulus tensor  $\mathbb{C}^\alpha$  is proportional to the tangent modulus tensor  $\mathbb{D}^\alpha$  such that  $2\mathbb{C}^\alpha = \mathbb{D}^\alpha$  so that

$$2 \frac{\partial \mathbb{C}^\alpha}{\partial \mathbf{C}^{\text{ve}}} = \frac{\partial \mathbb{D}^\alpha}{\partial \mathbf{C}^{\text{ve}}} = \mathbf{0} \quad (23)$$

This assumption is valid, since the St. Venant-Kirchhoff model is convex with respect to  $\mathbf{C}^{\text{ve}}$ . It should be noted, however, that some elastic energies that may not have convexity do not advocate this assumption [7]. Finally, with (18), (21) and (23), Eq. (17) can be written as

$$\mathbf{H} = \mathbf{H}^\infty + \sum_{\alpha=1}^{n_{\text{ve}}} [\gamma^\alpha \mathbf{H}^\infty - \mathbb{D}^\alpha : \boldsymbol{\Gamma}^\alpha] \quad (24)$$

The thermodynamic non-equilibrated stress that drives thermodynamic strain  $\boldsymbol{\Gamma}^\alpha$  is defined as  $\mathbf{R}^\alpha = -\rho_0 \frac{\partial \psi^{\text{ve}}}{\partial \boldsymbol{\Gamma}^\alpha}$  and its evolution equation can be derived with the internal dissipation energy (14) along the line of Holzapfel et al. [15, 16] as

$$\dot{\mathbf{R}}^\alpha + \frac{1}{\tau^\alpha} \mathbf{R}^\alpha = \frac{d}{dt} [\gamma^\alpha \mathbf{H}^\infty] - \mathbf{R}_{\text{cpl}} \quad (25)$$

where  $\tau^\alpha$  is the relaxation time of each Maxwell element, which is defined as a coefficient of the following relationship:

$$\mathbb{D}^\alpha : \dot{\boldsymbol{\Gamma}}^\alpha = \frac{1}{\tau^\alpha} \mathbf{R}^\alpha \quad (26)$$

Also,  $\mathbf{R}_{\text{cpl}}$  is the relaxation stress defined as

$$\mathbf{R}_{\text{cpl}} = \frac{D\mathbb{D}^\alpha}{Dt} : \boldsymbol{\Gamma}^\alpha \quad (27)$$

Here, since the components of  $\mathbb{D}^\alpha$  are constants, the relaxation stress in (27) is zero in this study. Thus, the thermodynamic non-equilibrated stress can be expressed as

$$\mathbf{R}^\alpha = \int_0^t \gamma^\alpha \frac{d\mathbf{H}^\infty}{ds} \exp\left[-\frac{s-t}{\tau^\alpha}\right] ds \quad (28)$$



Also, the thermodynamic strain  $\mathbf{\Gamma}^\alpha$  can be represented as

$$\mathbb{D}^\alpha : \mathbf{\Gamma}^\alpha = \gamma^\alpha \mathbf{H}^\infty - \mathbf{R}^\alpha \quad (29)$$

Finally, the substitution of (29) into (24) provides the non-equilibrated stress  $\mathbf{H}$  referring to  $B^{\text{vp}}$  as the sum of  $\mathbf{H}^\infty$  and  $\mathbf{R}^\alpha$  as

$$\mathbf{H} = \mathbf{H}^\infty + \sum_{\alpha=1}^{n_{\text{ve}}} \mathbf{R}^\alpha \quad (30)$$

## 2.4 Viscoplastic Rheology Element

The viscoplastic constitutive laws for amorphous thermoplastic resins must be capable of representing pseudo yielding followed by stress-softening in a small deformation regime and orientation hardening behavior in a large deformation regime.

### 2.4.1 Pseudo Yielding and Stress-Softening

The stress is exclusively determined in the viscoelastic rheology element described above and is applied to the viscoplastic rheology element, which is composed of viscoplastic slider and back-stress elements. Thus, the driving force acting on the viscoplastic slider element is the following effective stress referring to viscoelastically unloaded configuration  $B^{\text{vp}}$ :

$$\mathbf{M}^{\text{eff}} = \text{dev} (\mathbf{C}^{\text{ve}} \mathbf{H}(t) - \mathbf{M}^{\text{back}}) \quad (31)$$

Here,  $\mathbf{M}^{\text{back}}$  is the back stress. Defining the viscoplastic potential by  $\phi = \phi(\mathbf{M}^{\text{eff}}, \theta) = (\mathbf{M}^{\text{eff}} : \mathbf{M}^{\text{eff}})^{\frac{1}{2}}$ , we postulate the viscoplastic flow rule of the form

$$\bar{\mathbf{d}}^{\text{vp}} = \dot{\gamma}^{\text{vp}}(\theta) \mathbf{N}(\theta) \quad (32)$$

where  $\dot{\gamma}^{\text{vp}}$  is the viscoplastic multiplier, which is non-negative, and the flow vector has been defined as

$$\mathbf{N}(\theta) = \frac{\partial \phi}{\partial \mathbf{M}^{\text{eff}}} = \frac{1}{\sqrt{2}} \frac{\mathbf{M}^{\text{eff}}}{\tau} \quad (33)$$

Here,  $\tau$  is recognized as the equivalent stress of  $\mathbf{M}^{\text{eff}}$  defined as

$$\tau = \frac{1}{\sqrt{2}} \|\mathbf{M}^{\text{eff}}\| \quad (34)$$

As for the evolution equation of the viscoplastic multiplier, we employ the following phenomenological model, which was proposed by Boyce et al. [8] along the line of Argon [5] to represent pseudo yielding followed by stress softening in a relatively small deformation regime:

$$\dot{\gamma}^{\text{vp}}(\theta) = \dot{\gamma}_0^{\text{vp}} \exp \left[ -\frac{As^*}{\theta} \left\{ 1 - \left( \frac{\tau}{s^*} \right)^n \right\} \right] \quad (35)$$

where  $\dot{\gamma}_0^{\text{vp}}$  is the initial viscoplastic multiplier. Here, along with  $n$ ,  $A$  is the material parameter determined from the activation energy of Argon [5, 6] and is referred to as the activation volume. Also,  $s^*$  is a sort of yield strength representing the deformation resistance and has the following function form that depends on both the shear yield strength  $s$  and the hydrostatic pressure  $p = -\frac{1}{3} \text{tr}(\mathbf{C}^{\text{ve}} \mathbf{H})$ :

$$s^* = s + \alpha_v p \quad (36)$$

Here,  $\alpha_v$  is the pressure coefficient and the evolution law for  $s$  is postulated as

$$\dot{s} = h \left( 1 - \frac{s}{s_{\text{ss}}} \right) \dot{\gamma}^{\text{vp}} \quad (37)$$

where  $h$  is the inclination of the stress-softening response with respect to plastic strain after the initial yielding and  $s_{\text{ss}}$  is the shear yield strength in the steady state. Also, the athermal initial shear yield strength is introduced as  $s_0 = mG/(1-\nu)$ , where  $m$  is the material parameter associated with the activation energy. Here, we have used the shear modulus of elasticity defined as  $G = (1 + \sum_{\alpha}^{n_{\text{ve}}} \gamma^{\alpha}) G^{\infty}$  and Poisson's ratio  $\nu$  of the purely elastic element in the viscoelastic rheology element.

#### 2.4.2 Back Stress to Represent Orientation Hardening

When the conformation motion of a molecular chain transitions to the configuration motion due to its extension, the amorphous thermoplastic resin tends to exhibit an orientation hardening phenomenon, which has an analogy with the elastic behavior of rubber materials. Along the line of Ames et al. [2], we employ the following Gent's hyperelastic energy function [14] to represent the orientation hardening.

$$\rho_0 \psi^{\text{vp}} = -\frac{1}{2} \mu J_m \ln \left( 1 - \frac{I_1 - 3}{J_m} \right) \quad (38)$$

Here,  $I_1 = \text{tr}(\bar{\mathbf{b}}^{\text{vp}})$  is the first invariant of the viscoelastic left-Cauchy-Green deformation tensor  $\bar{\mathbf{b}}^{\text{vp}}$ ,  $J_m$  is the characteristic length of extended molecular chains, which is supposed to satisfy  $J_m > I_1 - 3$ . Also,  $\mu$  is the shear modulus-like material parameter associated with the back stress. Then, it can be derived as

$$\mathbf{M}^{\text{back}} = 2\rho_0 \frac{\partial \Psi^{\text{vp}}}{\partial \bar{\mathbf{b}}^{\text{vp}}} \bar{\mathbf{b}}^{\text{vp}} = \mu \left( 1 - \frac{I_1 - 3}{J_m} \right)^{-1} \bar{\mathbf{b}}^{\text{vp}} \quad (39)$$

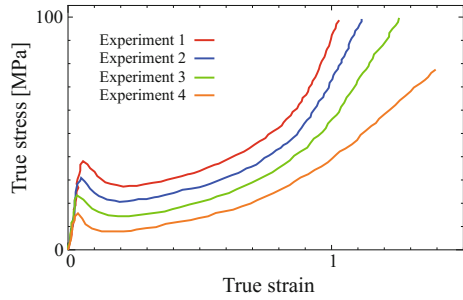
### 3 Identification of Material Parameters

The set of constitutive equations proposed in this study is summarized in Fig. 3. This section is devoted to the identification of the material parameters used in these equations. The experimental data are borrowed from Hope et al. [17] who conducted a series of uniaxial tension tests for PMMA with different deformation rates. The tests were carried out with four levels of true strain rates 0.1, 0.01, 0.001 and 0.0001 s at ambient temperature of 90 °C . The obtained empirical relationships between true stresses and true strains are shown in Fig. 4. Although the maximum tensile strain attains 1.5, the parameter identification in this study is made for the data up to true strain of 1.0.

[1] Kinematic variables		(4) Thermomechanical non-equilibrium stress	
(1) Multiplicative decomposition of total deformation gradient	$\mathbf{F} = \bar{\mathbf{F}}\mathbf{F}^{\text{th}}$	(5) Tangent modulus of ideal elasticity tensor of Maxwell element	$\mathbb{D} = \gamma^\alpha (K^\infty \mathbf{I}^{\text{sym}} + 2G\mathbf{I}^{\text{dev}})$
(2) Thermal dilatation deformation gradient	$\mathbf{F}^{\text{th}} = (1 + \alpha_t \theta)\mathbf{1}$	[3] Viscoplasticity	
(3) Multiplicative decomposition of mechanical deformation gradient	$\bar{\mathbf{F}} = \mathbf{F}^{\text{ve}}\bar{\mathbf{F}}^{\text{vp}}$	(1) Viscoplastic hardening law	$\bar{\mathbf{d}}^{\text{vp}} = \dot{\gamma}^{\text{vp}} \frac{\mathbf{M}^{\text{eff}}}{\ \mathbf{M}^{\text{eff}}\ }$
(4) Viscoelastic right Cauchy-Green tensor	$\mathbf{C}^{\text{ve}} = (\mathbf{F}^{\text{ve}})^\top \mathbf{F}^{\text{ve}}$	(2) Effective deviatoric stress	$\mathbf{M}^{\text{eff}} = \text{dev}(\mathbf{C}^{\text{ve}}\mathbf{H} - \mathbf{M}^{\text{back}})$
(5) Viscoplastic left Cauchy-Green tensor	$\bar{\mathbf{b}}^{\text{vp}} = \bar{\mathbf{F}}^{\text{vp}}(\bar{\mathbf{F}}^{\text{vp}})^\top$	(3) Back stress	$\mathbf{M}^{\text{back}} = \mu \left( 1 - \frac{I_1^{\text{vp}}}{J_m} \right)^{-1} \bar{\mathbf{b}}^{\text{vp}}$
(6) Viscoelastic Green-Lagrange strain tensor	$\mathbf{E}^{\text{ve}} = \frac{1}{2}(\mathbf{C}^{\text{ve}} - \mathbf{1})$	(4) Evolution law of viscoplastic multiplier	$\dot{\gamma}^{\text{vp}} = \dot{\gamma}_\sigma^{\text{vp}} \exp \left[ -\frac{\Delta S^*}{\theta} \left( 1 - \frac{\ \mathbf{M}^{\text{eff}}\ ^2}{\sqrt{2} s^*} \right) \right]$
(7) Viscoplastic velocity Gradient tensor	$\bar{\mathbf{T}}^{\text{vp}} = \bar{\mathbf{d}}^{\text{vp}} + \dot{\bar{\mathbf{w}}}$	(5) Yield strength	$s^* = s - \frac{\alpha_s}{3} \text{tr}(\mathbf{C}^{\text{ve}}\mathbf{H})$
(8) Mechanical spin tensor	$\dot{\bar{\mathbf{w}}} = \text{skew}(\dot{\bar{\mathbf{F}}}\bar{\mathbf{F}}^{-1})$	(6) Evolution law of shear yield strength	$\dot{s} = h \left( 1 - \frac{s}{s_s} \right) \dot{\gamma}^{\text{vp}}$
[2] Viscoelasticity		(7) Athermal initial shear yield strength	$s_0 = m \frac{G}{1-\nu}$
(1) 2nd Piola-Kirchhoff real stress	$\mathbf{S} = (\bar{\mathbf{F}}^{\text{vp}})^{-1} \mathbf{H}(\bar{\mathbf{F}}^{\text{vp}})^{-\top}$		
(2) Real stress	$\mathbf{H} = \mathbf{H}^\infty + \sum_{\alpha=1}^{n_{bc}} \mathbf{R}^\alpha$		
(3) Pure elastic stress	$\mathbf{H}^\infty = K^\infty \text{tr}(\mathbf{E}^{\text{ve}})\mathbf{1} + 2G\text{dev}(\mathbf{E}^{\text{ve}})$		

Fig. 3 Summary of the proposed constitutive model

**Fig. 4** Experimental data of the uniaxial tensile test in Hope et al. [17]. The data shows the relationship between the true stress and true strain for 4 levels of deformation rates; “0.1, 0.01, 0.001, 0.0001 (/s)” under temperature 90°



It should be noted that the relaxation times and CTE can hardly be identified with the referential experimental data. Therefore, these parameters are assumed as in Table 1, where the number of Maxwell elements are presumably set at 18. Thus, the number of unknown parameters to be identified is 27, which counts eighteen relative elastic moduli in the generalized Maxwell model.

The method of differential evolution (DE) is used for meta-heuristic optimization of the material parameters. Displacement is imposed on the end nodes of a cubic single eight-node hexahedral element with dimension of  $1.0 \times 1.0 \times 1.0 \text{ mm}^3$  for each tensile test with a specified strain rate. The boundary condition is set to realize the uniform uniaxial stress state. Then all the calculated relationships between true stresses and true strains are compared with experimental ones provided in Fig. 4.

The material parameters thus determined are presented in Tables 2 and 3. Figure 5 shows the corresponding curves representing relationships between true stresses and true strains. As can be seen from the figure, the stress softening behavior after the initial yielding can be captured, as the viscoelastic model of Boyce et al. [8] employed

**Table 1** Fixed parameters

Maxwell elements	CTE (1/°C)	Relaxation time (s)
18	$5.0 \times 10^{-5}$	$10^x$ (x are integers from 1 to 18)

**Table 2** Identified parameters

Parameter	Value
$E$ (MPa)	2061
$\nu$	0.3772
$\dot{\gamma}_0^{vp}$ (/s)	$1.145 \times 10^{11}$
$A$ (K/MPa)	166
$\alpha$	0.2289
$h$ (MPa)	844.6
$s_{ss}$ (MPa)	81.55
$J_m$	22.28
$\mu$ (MPa)	4.651

**Table 3** Identified relative elastic moduli

$\alpha$	Value	$\alpha$	Value
1	$1.328 \times 10^{-3}$	10	$2.818 \times 10^{-2}$
2	$2.174 \times 10^{-3}$	11	$1.930 \times 10^{-2}$
3	$2.974 \times 10^{-3}$	12	$7.350 \times 10^{-2}$
4	$1.674 \times 10^{-3}$	13	$3.400 \times 10^{-2}$
5	$1.106 \times 10^{-4}$	14	$2.642 \times 10^{-2}$
6	$5.612 \times 10^{-3}$	15	$2.707 \times 10^{-2}$
7	$3.951 \times 10^{-4}$	16	$4.294 \times 10^{-2}$
8	$1.139 \times 10^{-2}$	17	$8.415 \times 10^{-3}$
9	$2.290 \times 10^{-2}$	18	$9.351 \times 10^{-2}$

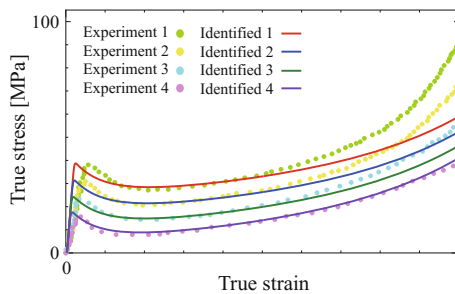


**Fig. 5** Identification results. The result successfully captures the stress softening after quasi-yielding and followed by the orientation-hardening phenomenon. However, in all the cases, the initial elastic regime deviate from the experimental one and the hardening progresses in a large deformation regime are almost in parallel. These discrepancies must be due to the lack of the data of dynamic viscoelastic behavior

in the proposed model takes into account the variation of the shear yield strength. However, since the time-variation of the free volume caused by molecular chain slippage is not considered, the calculated curves lack the smoothness of the softening behavior around the upper yielding points. Also, the orientation hardening can be represented thanks to the introduction of the back stress, though the representation of the effect of extended chains are insufficient. This discrepancy is probably due to the fact that the viscoplastic deformation rates of all the rate levels are almost the same in a large strain regimes and so are the evolutions of the back stresses that depends on the viscoplastic deformation. The improvement of these performances are future subjects of study.

Finally, in order to reflect the temperature-dependent behavior and viscoelastic characteristics in the proposed model, we need more tensile test results with different temperature levels, dynamic viscoelastic measurements and strain recovery tests. It is therefore to be noted that the material behavior presented in this study with the assumed material parameters are not relevant to these properties and cannot be representative of actual thermoplastic materials.

## 4 Numerical Examples

Using the proposed constitutive laws with the material parameters determined in the previous section, we demonstrate the fundamental material behavior that can be represented by the proposed constitutive model.

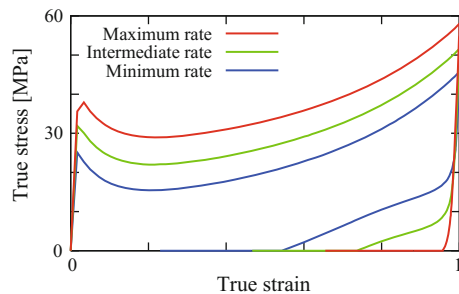
### 4.1 Behavior Under Loading, Unloading and Uncontrolled States

With the same single element model used for the parameter identification in the previous section, consecutive uniaxial responses under loading, unloading and uncontrolled conditions are demonstrated. Three levels of deformation rates at ambient temperature of 90 °C are considered in this example. The corresponding analysis cases are labelled as Maximum, Intermediate and Minimum Cases in the order of the rates. For Maximum Case, the single element is subjected to loading in the first 10 s, unloading in the next 10 s and then uncontrolled for the last 30 s. For Intermediate and Minimum Cases, the time intervals are 10 and 100 times longer than the maximum case, respectively. In each of these analysis cases, the maximum tensile true strain is set to be 1.0.

Figure 6 shows the calculated relationships between true stresses and true strains. As can be recognized from this figure, the yielding behavior depends on the deformation rates; that is, the higher the initial yield stress, the higher the deformation rate. Also, after the stress softening, all the stress responses evolve in the same manner. Specifically, the stresses are increased at the same rate so that the curves are almost parallel. This is probably due to the fact that the evolution rates of the viscoplastic multiplier are the same for all the cases, implying that the evolution rates of the shear yielding strength  $s^*$  are the same regardless of deformation rates.

In the unloading process, the higher the deformation rate, the larger the inclination. More specifically, the stress in Maximum Case is almost linearly decreased and only a small amount of strain is recovered by the stress-free state. This is due the fact that, as the deformation rate becomes lower, the inelastic deformation becomes

**Fig. 6** Relationships between true stresses and true strains obtained under tensile loading, unloading and uncontrolled conditions



more prominent during the unloading process. On the other hand, as the deformation rate becomes lower in the unloading process, the curves are more gently inclined. In fact, almost half of the total true strain is recovered in Minimum Case. This is due to the viscoplastic deformation in the unloading process caused by the residual stress. These responses in the unloading process are not consistent with the experimental evidence reported in the literature (see, for example, Srivastava et al. [30]) and the discrepancy must be due to the assumed values of viscoelastic material parameters such as elastic moduli and relaxation times.

In the uncontrolled process with the external loading being zero, the amount of strain recovery is the same for all the cases, implying that the corresponding residual stresses due to viscoelastic deformation are comparable. Although this kind of strain recovery is always observed in experiments with cyclic loading, few existing constitutive models for amorphous thermoplastic resins direct attention towards the representation of strain recovery along with viscoplastic characteristics.

To study the underlining mechanisms of the above-mentioned apparent behavior, we provide the variations of viscoelastic non-equilibrated stresses in some Maxwell elements in Fig. 7 Here, we have chosen elements No. 12, 16, 17 and 18, as they exhibit relatively large viscoelastic stresses. First, in the loading process, the dominant stress responses in each of the subfigures are similar to those of the total

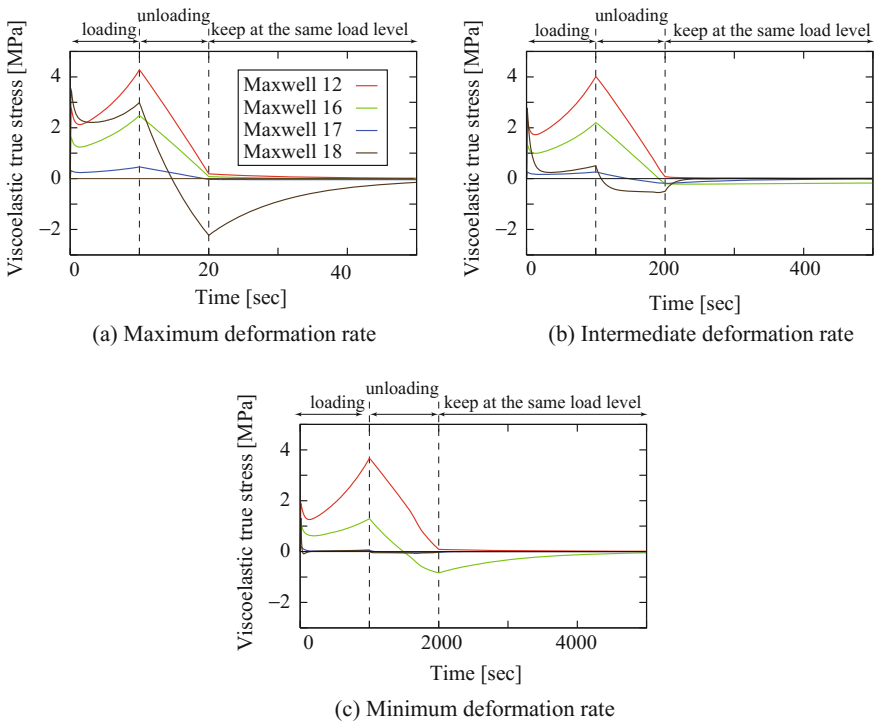


**Fig. 7** Thermomechanical viscoelastic stresses of Maxwell elements

true stresses depicted in Fig. 6. This must be due to the fact that the stress in the proposed constitutive model is realized only in the set of viscoelastic rheology elements and directly affected by viscoplastic flow and back stress. Also, in the unloading process, most of the viscoelastic stresses are decreased in an almost linear manner, but some of them exhibit negative or compressive values, even though the total stress are positive. Then, these negative stresses remain when the external loading becomes zero and gradually relaxed in the uncontrolled process. Thus, the main sources of the residual stress that plays a driving force for the strain recovery mentioned above must be these negative viscoelastic stresses.

In addition, element No. 12 and 16 are active in all the cases. However, element No. 17 and 18 contribute the total stress in Maximum Case, while the effect of element No. 18 disappears in Intermediate Case. Moreover, both the effects of element No. 17 and 18 are not negligible in Minimum Case. These viscoelastic responses that depend on deformation rate are relevant to the relationship between relaxation time and time rate of change of deformation. In fact, the time spent in the loading process of Maximum Case is 10 s, which is comparable with the relaxation time of element No. 18. It is reasonable for Maxwell's elements with short relaxation times to respond to higher rates of deformation.

#### ***4.2 Stress Relaxation and Strain Recovery in a Standard Specimen***

Using the same material parameters determined above, we carry out two simulations of uni-axial tests for a standard specimen shown in Fig. 8 to demonstrate the capability of the proposed constitutive model. One of them is a stress relaxation test and the other is a strain recovery test. The finite element (FE) model used here is composed of 2160 eight-node hexahedral elements with 3597 nodes and one-quarter of the specimen. The maximum elongation in the loading process is set at 60 mm for both of the simulations and the ambient temperature of 50 °C is kept constant during the entire process.

For both cases of numerical simulations, the specimen is loaded in 10 s. Then the elongation of 60 mm is kept for 10 s in the stress relaxation case. In the strain recovery case, the reaction force at the end section is reduced to zero in 10 s and the specimen is left untouched for 10 s. Figures 9 and 10 show the time-variations of the apparent stress and the relationships between true stress and strain for the stress relaxation and strain recovery cases, respectively. Here, the apparent stress is defined as the reaction force divided by the end section area of the specimen, which is referred to as nominal stress in this study. On the other hand, the true stress and strain are measured at the center of element A indicated in Fig. 8. In these figure, State (F) corresponds to the end of the loading, while (L) in Fig. 9 and (J) in Fig. 10 correspond the ends of the processes of stress relaxation and strain recovery, respectively.



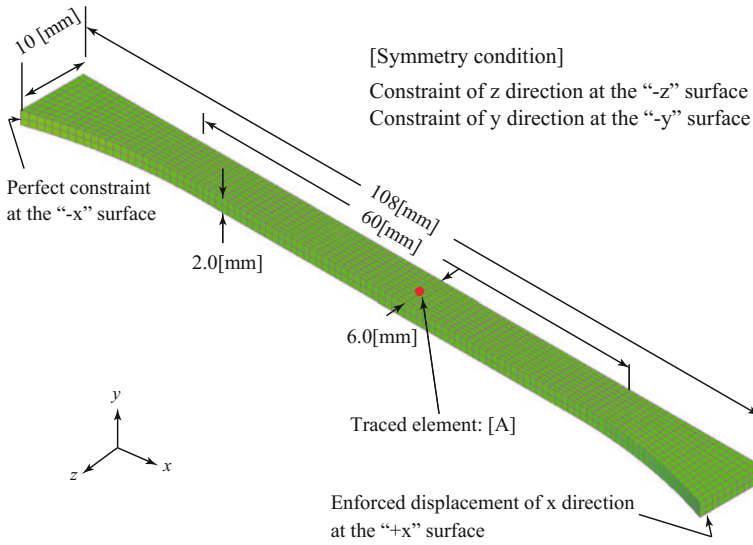


**Fig. 8** Tensile specimen model with spatial dimension and boundary conditions

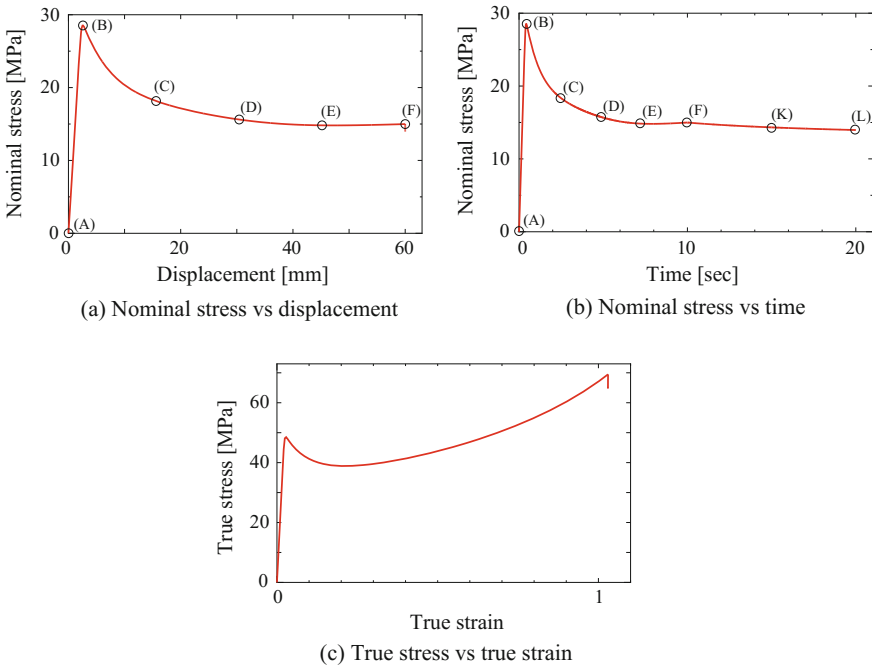


**Fig. 9** Analysis results of stress relaxation test: **a** Relationship between nominal stress and enforced displacement; **b** Relationship between nominal stress and time; **c** Relationship between true stress and true strain

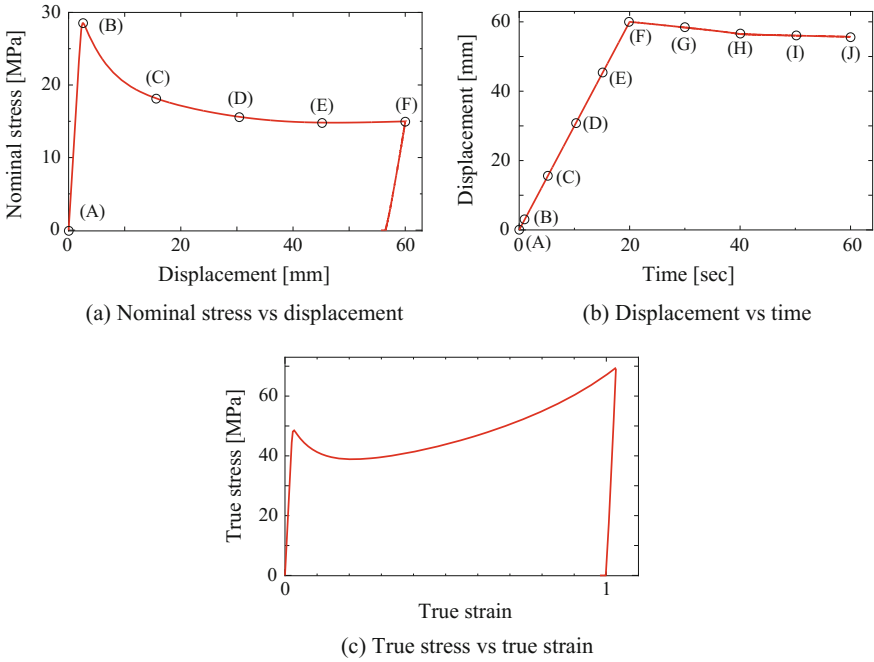


**Fig. 10** Analysis results of strain recovery test: **a** Relationship between nominal stress and enforced displacement; **b** Relationship between enforced displacement and time; **c** Relationship between true stress and true strain

**Fig. 11** Deformed configurations with von-Mises equivalent stress distributions in the tensile specimen of during loading process

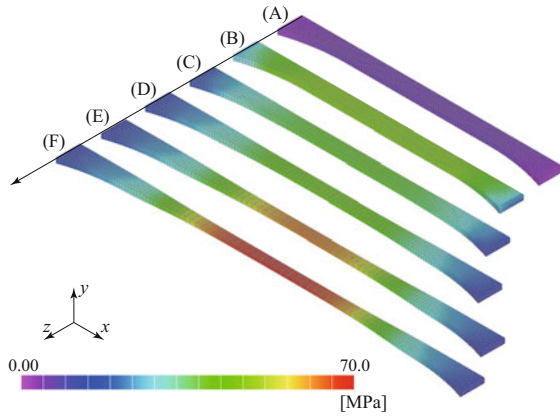
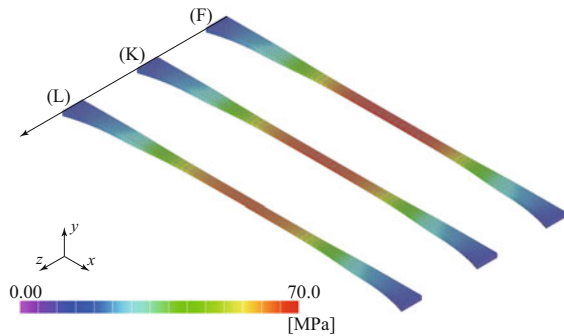


Figure 11 shows the deformed configurations with the distributions of von-Mises stresses at six deformation states calculated in the loading process. As can be seen in the figure, when the specimen reaches a moderate deformation level, the necking phenomenon becomes visible around the central part of the specimen, which is

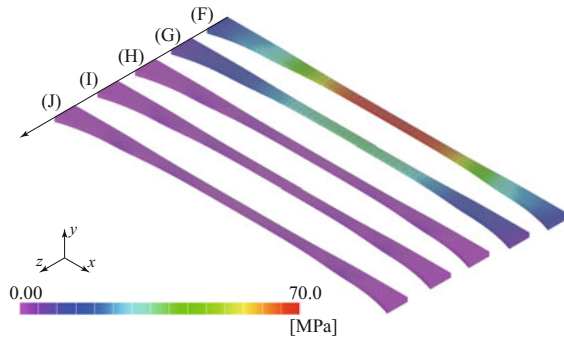
followed by the stress concentration due to large deformation. The subsequent deformed configurations with the von-Mises stress distributions are shown in Fig. 12 for the stress relaxation case and Fig. 13 for the strain recovery case, in which each of the deformed configurations corresponds to the state indicated in Figs. 9 and 10.

The deformation process from States (A)–(F) depicted in Fig. 11 is common to both the stress relaxation and strain recovery cases. In State (B) at the beginning of tensile deformation, both the apparent and true stresses attain their maximum values and then decrease towards State (C). Although the decrease in the apparent stress here is also typical in standard specimens of metals, the decrease in the true stress is unique to the mechanical behavior of amorphous thermoplastic resins. It is, however, known that, in actual experiments, the specimen exhibits the localization of viscoplastic strain due to necking at the central part of the specimen and its region expands towards the end section during the stress softening behavior after the initial yielding. The proposed model is capable of representing stress softening, but not such localization phenomena. In fact, the necking starts after State (D) of moderate deformation in our numerical simulation. As can be seen in (E) and (F) of (c) in Figs. 9 and 10, the orientation hardening is observed in the true stress at the last stage of the loading process. This has also been demonstrated in the previous subsection. In these states of deformation, the stress is concentrated around the central part of

**Fig. 12** Deformed configurations with the von-Mises equivalent stress distributions in tensile specimen during sustained tensile process in stress relaxation case



**Fig. 13** Deformed configurations with von-Mises equivalent stresses distributions in the tensile specimen of during unloading and sustaining processes in strain recovery case



the specimen. On the contrary, the apparent stress is not affected by such hardening behavior and provides almost constant level reflecting only the resistance against the viscoplastic flow.

The deformed configurations with stress distributions from States (F)–(L) for the stress relaxation case, which is illustrated in Fig. 12, show that the stress relaxation is observed in the whole part of the specimen, but predominant around the central part of the specimen. However, the amount of stress relaxation is small, because the sustained period of constant elongation was set short.

For the strain recovery case, the whose deformation states during unloading and sustaining processes are illustrated in Fig. 13. In the unloading process, which corresponds to States (G) and (H), the nominal and true stresses significantly decrease due to the rapid recovery of elastic springs of each Maxwell element. As can be seen from Fig. 10, some of the Maxwell elements are supposed to be non-equilibrated in State (I) in Fig. 13 and then equilibrated in State (J) so that a small strain is recovered in the sustaining process.

Both the stress transitions and deformation states have been obtain as we originally intended. It should be noted that the stress relaxation and strain recovery responses simulated here are attributed to the coupling between viscoelasticity and viscoplasticity whose rheology elements are aligned in series. However, mainly due to inadequate parameter setting, the extents of stress relaxation and strain recovery are scarce. Also, there must be some room for improvement in function forms of the constitutive laws.

## 5 Conclusion

We have proposed a viscoelastic-viscoplastic combined constitutive model for amorphous thermoplastic resins within the finite strain framework. The simple rheology model introduced consisted of viscoelastic and viscoplastic elements connected in series. The standard generalized Maxwell model was used to determine the stress and characterize the viscoelastic material behavior at small or moderate strain regimes. On the other hand, we employed a proven finite strain viscoplastic model to realize the creep deformations along with the kinematic hardening behavior due to orientation of molecular chains. After the material parameters were identified with reference to experimental data, the fundamental performances of the proposed model were verified in representative numerical examples. In particular, it has been confirmed that the proposed model is capable of reproducing stress softening and strain recovery simultaneously.

However, due to the lack of experimental data that consistently represent both viscoelastic and viscoplastic responses, the quantitative agreement with the actual material behavior could not be confirmed. Indeed, a simple viscoplastic model seems not to have adequate performance in reflecting the limiting extensibility of polymer chains. Also, the identification accuracy of the viscoelastic spectral characteristics was not satisfactory and accordingly the strain recovery phenomenon were unreal-

istic. Nonetheless, it was our original contribution that the elastic characteristics of thermoplastic resins were totally taken by the set of viscoelastic rheology elements because of the connection of these two separate rheology elements in series.

Of course, various improvements must be introduced to our model. For example, the present model neglects the dependencies of the elastic and orientation hardening responses on temperature. It is also known that viscoelastic properties of amorphous thermoplastic resins become prominent when microscopic Brownian motions of molecular chains become active around the glass transition temperature and when pseudo chemical crosslink is constructed by the change in molecular chain orientation caused by crystallization. Thus, the rubber-like material behavior must appear above the glass-transition temperature. It remains a challenge for future research to incorporate these temperature dependencies.

## References

1. N. Aleksy, G. Kermouche, A. Vautrin, J.M. Bergheau, Numerical study of scratch velocity effect on recovery of viscoelastic-viscoplastic solids. *Int. J. Mech. Sci.* **52**, 455–463 (2010)
2. N.M. Ames, V. Srivastava, S.A. Chester, L. Anand, A thermo-mechanically coupled theory for large deformations of amorphous polymers. part II: applications. *Int. J. Plast.* **25**, 1495–1539 (2009)
3. L. Anand, N.M. Ames, V. Srivastava, S.A. Chester, A thermo-mechanically coupled theory for large deformations of amorphous polymers. part I: formulation. *Int. J. Plast.* **25**, 1474–1494 (2009)
4. L. Anand, M.E. Gurtin, A theory of amorphous solids undergoing large deformations with application to polymeric glasses. *Int. J. Solids Struct.* **40**, 1465–1487 (2003)
5. A.S. Argon, A theory for the low-temperature plastic deformation of glassy polymers. *Philos. Mag.* **28**, 839–865 (1973)
6. A.S. Argon, *The Physics of Deformation and Fracture of Polymers* (Cambridge University Press, Cambridge, New York, USA, 2013)
7. J.M. Ball, Convexity conditions and existence theorems in nonlinear elasticity. *Arch. Ration. Mech. Anal.* **63**, 337–403 (1976)
8. M.C. Boyce, D.M. Parks, A.S. Argon, Large inelastic deformation of glassy polymers. part I: rate dependent constitutive model. *Mech. Mater.* **7**, 15–33 (1988)
9. R.B. Dupaix, M.C. Boyce, Constitutive modeling of the finite strain behaviour of amorphous in and above the glass transition. *Mech. Mater.* **39**, 39–52 (2007)
10. H. Eyring, Viscosity, plasticity, and diffusion as examples of absolute reaction rates. *J. Chem. Phys.* **4**, 283 (1936)
11. R. Fleischhauer, H. Dal, M. Kaliske, K. Schneider, A constitutive model for finite deformation of amorphous polymers. *Int. J. Mech. Sci.* **65**, 48–63 (2012)
12. P.J. Flory, Thermodynamic relations for high elastic materials. *Trans. Faraday Soc.* **57**, 829–838 (1961)
13. D.G. Fotheringham, B.W. Cherry, The role of recovery forces in the deformation of linear polyethylene. *J. Mater. Sci.* **13**, 951–964 (1978)
14. A.N. Gent, A new constitutive relation for rubber. *Rubber Chem. Technol.* **69**, 59–61 (1996)
15. G.A. Holzapfel, J.C. Simo, A new viscoelastic constitutive model for continuous media at finite thermomechanical changes. *Int. J. Solids Struct.* **33**, 3019–3034 (1996)
16. G.A. Holzapfel, *Nonlinear Solid Mechanics a Continuum Approach for Engineering* (Wiley) (2000)

17. P.S. Hope, I.M. Ward, A.G. Gibson, The hydrostatic extrusion of polymethylmethacrylate. *J. Mater. Sci.* **15**, 2207–2220 (1980)
18. G. Kermouche, N. Aleksey, J.M. Bergheau, Viscoelastic-viscoplastic modelling of the scratch response of PMMA. *Adv. Mater. Sci. Eng.* **2013** (2013), Article ID 289698
19. E. Kröner, Allgemeine kontinuumstheorie der versetzungen und eigenspannungen. *Arch. Ration. Mech. Anal.* **4**, 273–334 (1960)
20. E.H. Lee, Elastic plastic deformation at finite strain. *J. Appl. Mech.* **36**, 16 (1969)
21. J.C.M. Li, J.J. Gilman, Disclination loops in polymers. *J. Appl. Phys.* **41**, 4248–4256 (1970)
22. G.C.T. Liu, J.C.M. Li, Strain energies of disclination loops. *J. Appl. Phys.* **42**, 3313–3315 (1971)
23. A.D. Mulliken, M.C. Boyce, Mechanics of the rate-dependent elastic-plastic deformation of glassy polymers from low to high strain rates. *Int. J. Solids Struct.* **43**, 1331–1356 (2006)
24. B. Nedjar, Frameworks for finite strain viscoelastic-plasticity based on multiplicative decompositions. part I: continuum formulations. *Comput. Methods Appl. Mech. Eng.* **191**, 1541–1562 (2002a)
25. B. Nedjar, Frameworks for finite strain viscoelastic-plasticity based on multiplicative decompositions. part II: computational aspects. *Comput. Methods Appl. Mech. Eng.* **191**, 1563–1593 (2002b)
26. E.A. de Neto Souza, D. Peric, D.R.J. Owen, *Computational Methods for Plasticity: Theory and Applications* (Wiley, Chichester, West Sussex, UK, 2008)
27. J. Richeton, S. Ahzi, L. Daridon, Y. Remond, A formulation of the cooperative model for the yield stress of amorphous polymers for a wide range of strain rates and temperatures. *Polymer* **46**, 6035–6043 (2005)
28. J. Richeton, S. Ahzi, K.S. Vecchio, F.C. Jiang, R.R. Adharapurapu, Influence of temperature and strain rate on the mechanical behavior of three amorphous polymers: Characterization and modeling of the compressive yield stress. *Int. J. Solids Struct.* **43**, 2318–2335 (2006)
29. J. Richeton, S. Ahzi, K.S. Vecchio, F.C. Jiang, A. Makradi, Modeling and validation of the large deformation inelastic response of amorphous polymers over a wide range of temperatures and strain rates. *Int. J. Solids Struct.* **44**, 7938–7954 (2007)
30. V. Srivastava, S.A. Chester, N.M. Ames, L. Anand, A thermo-mechanically-coupled large-deformation theory for amorphous polymers in a temperature range which spans their glass transition. *Int. J. Plast.* **26**, 1138–1182 (2010)
31. P.D. Wu, E.V.D. Giessen, Analysis of shear band propagation in amorphous glassy polymers. *Int. J. Solids Struct.* **31**, 1493–1517 (1994)
32. P.D. Wu, E.V.D. Giessen, On neck propagation in amorphous glassy polymers under plane strain tension. *Int. J. Plast.* **11**, 211–235 (1995)